Discovery and preclinical evaluation of a novel class of small-molecule compounds in hormone-dependent and -independent cancer cell lines

Carmen Plasencia,[1] Raveendra Dayam,[1] Qingcai Wang,[2] Jacek Pinski,[2] Terrence R. Burke, Jr.,[3] David I. Quinn,[2] and Nouri Neamati[1]

[1]Department of Pharmaceutical Sciences, School of Pharmacy, University of Southern California; [2]Department of Medicine, Keck School of Medicine, University of Southern California, Norris Comprehensive Cancer Center, Los Angeles, California; and [3]Laboratory of Medicinal Chemistry, Center for Cancer Research, NIH, Frederick, Maryland

Abstract

We discovered a series of salicylhydrazide class of compounds with remarkable anticancer activity against a panel of hormone receptor–positive and -negative cell lines. In the present study, we evaluated the *in vitro* activity of SC21 and SC23 against a range of human tumor cell types and the *in vivo* efficacy of compound SC21 in a PC3 human prostate cancer xenograft model in mice. We also determined the effects of SC21 on cell cycle regulation and apoptosis. Our *in vitro* results show that salicylhydrazides are highly potent compounds effective in both hormone receptor–positive and -negative cancer cells. SC21 induced apoptosis and blocked the cell cycle in G_0/G_1 or S phase, depending on the cell lines used and irrespective of p53, p21, pRb, and p16 status. SC21 effectively reduced the tumor growth in mice without apparent toxicity. Although the mechanism of action of SC21 is not completely elucidated, the effect on cell cycle, the induction of apoptosis and the activity against a panel of tumor cell lines of different origins prompted us to carry out an in-depth preclinical evaluation of SC21. [Mol Cancer Ther 2005;4(7):1105–13]

Introduction

There is a desperate need to develop highly active, well-tolerated, and easy to use (ideally orally active) drugs, which exploit our increased understanding of tumor biology. However, one major hurdle to overcome in a drug discovery program is the identification of a suitable lead compound having desired biological activity. Less than 1% of tested compounds will eventually become selected for further studies. Preclinical evaluation of pharmacokinetic and pharmacodynamic properties and a knowledge of drug metabolism are important in the drug development processes. After a drug candidate is selected for further study, detailed information from *in vitro* screening as well as an evaluation of *in vivo* efficacy and toxicity in animal models is required to predict the *in vivo* outcome of selected compounds in humans. Traditional pharmacokinetic studies, although essential, are cumbersome and time-consuming and require a large number of animals. Recent technological advances in computer simulations have allowed absorption, distribution, metabolism, excretion, and toxicity (ADMET) prediction to become a reliable and rapid means of decreasing the time and resources needed to evaluate the therapeutic potential of a drug candidate (1).

Previously, we showed that certain of our HIV-1 integrase inhibitors exhibit significant cytotoxicity due to lack of selectivity for integrase (2–5). In fact, the similarities between retroviral integrases and topoisomerase prompted the first study that evaluated topoisomerase I and II poisons against integrase (6). As a result, we have been routinely using topoisomerases as a counter screen for integrase inhibitors (4, 5, 7–9). In a more recent study, we showed that even the most selective integrase inhibitors identified thus far also inhibit RAG1/2 enzymes that are essential for VDJ recombination (10). All these enzymes share a similar chemistry of DNA binding, DNA cleavage, and recombination that require divalent metal (Mn^{2+} and Mg^{2+} but not Ca^{2+}; ref. 11). Because integrase belongs to a large family of polynucleotidyl transferases (12), it is plausible that certain of our inhibitors could target an unknown DNA-processing enzyme.

Accordingly, we built a 10,000 compound database of reported and patented integrase inhibitors, which are in some instances likely to target additional DNA processing enzymes, possibly even more potently than integrase. Using this database, we developed various pharmacophore models followed by toxicity prediction using ADMET Predictor software package (Simulations Plus, Inc., Lancaster, CA) and cluster analysis to separate a majority of antiviral compounds from cytotoxics.[4] On the basis of these pharmacophores, we identified the salicylhydrazide class of compounds as potential leads for inclusion in our

Received 10/28/04; revised 4/20/05; accepted 5/4/05.

Grant support: The Susan G. Komen Breast Cancer Foundation, Gustavus and Louise Pfeiffer Research Foundation, University of Southern California School of Pharmacy and Norris Cancer Center (to N. Neamati).

The costs of publication of this article were defrayed in part by the payment of page charges. This article must therefore be hereby marked advertisement in accordance with 18 U.S.C. Section 1734 solely to indicate this fact.

Requests for reprints: Nouri Neamati, Department of Pharmaceutical Sciences, School of Pharmacy, University of Southern California, 1985 Zonal Avenue, Los Angeles, CA 90089. Phone: 323-442-2341; Fax: 323-442-1390. E-mail: neamati@usc.edu

[4] N. Neamati, C. Plasencia, and R. Dayam, unpublished.

anticancer drug discovery program. Pursuing development of this class of compounds, we searched our in-house multiconformational database of ~4.5 million compounds and identified >2,200 compounds that possess common structural features and pharmacophore fragments. We then acquired 950 analogues from commercial sources and subjected them to 3-(4,5-dimethylthiazol-2-yl)-2,5-diphenyltetrazolium bromide cytotoxicity assays for an initial screen followed by in-depth testing of proprietary derivatives. An additional 740 compounds that did not satisfy our ADMET calculations were not tested.

Herein, we present the activity profiles of 18 of these compounds *in vitro* and focus on two compounds, SC21 and SC23, for detailed analyses. Our results indicate that SC21 and SC23 show remarkable activity in a panel of tumor cell lines, including androgen receptor–positive and -negative prostate cancer cells, estrogen receptor–positive and -negative breast cancer cells and an ovarian cancer line intrinsically resistant to cisplatin. Additionally, we tested the effects of SC21 on cell cycle regulation and apoptosis and evaluated the *in vivo* therapeutic potential of SC21 in a human prostate cancer xenograft model.

Materials and Methods

Cell Culture

Human prostate cancer cells (PC3, p53 null, AR−; DU145, p53 mutant, AR−; and LNCaP, p53 wild-type, AR+) and breast cancer cells (MCF-7, overexpressed wild-type p53, ER+; MDA-MB-468, p53 mutant, ER+; and MDA-MB-435, p53 mutant, ER−) were obtained from the American Type Cell Culture (Manassas, VA). The human ovarian carcinoma cell line (HEY) naturally resistant to cisplatin (CDDP) was kindly provided by Dr. Dubeau (University of Southern California Norris Cancer Center; refs. 13, 14). The results with CEM cells were previously described (4). Cells were maintained as monolayer cultures in RPMI 1640 supplemented with 10% fetal bovine serum (Gemini-Bioproducts, Woodland, CA) and 2 mmol/L L-glutamine at 37°C in a humidified atmosphere of 5% CO_2. To remove the adherent cells from the flask for passaging and counting, cells were washed with PBS without calcium or magnesium, incubated with a small volume of 0.25% trypsin-EDTA solution (Sigma-Aldrich, St. Louis, MO) for 5 to 10 minutes, and washed with culture medium and centrifuged. All experiments were done using cells in exponential cell growth.

Drugs

A 10 mmol/L stock solution of all compounds were prepared in DMSO and stored at −20°C. Further dilutions were freshly made in PBS.

Cytotoxicity Assay

Cytotoxicity was assessed by a 3-(4,5-dimethylthiazol-2-yl)-2,5-diphenyltetrazolium bromide assay as previously described (15). Briefly, cells were seeded in 96-well microtiter plates (PC3 and DU145 at 5,000 cells/well and LNCaP at 10,000 cells/well; breast and ovarian cells at 4,000 cells/well) and allowed to attach. Cells were subsequently treated with a continuous exposure to the corresponding drug for 72 hours. A 3-(4,5-dimethylthiazol-2-yl)-2,5-diphenyltetrazolium bromide solution (at a final concentration of 0.5 mg/mL) was added to each well and cells were incubated for 4 hours at 37°C. After removal of the medium, DMSO was added and the absorbance was read at 570 nm. All assays were done in triplicate. The IC_{50} was then determined for each drug from a plot of log (drug concentration) versus percentage of cell kill.

Cell Cycle Analysis

Cell cycle perturbations induced by SC21 and camptothecin (CPT) were analyzed by propidium iodide DNA staining. Briefly, exponentially growing PC3 and DU145 cells were treated with different doses of the drug for 24, 48, and 72 hours. At the end of each treatment time, cells were collected and washed with PBS after a gentle centrifugation at 200× *g* for 5 minutes. Cells were thoroughly resuspended in 0.5 mL of PBS and fixed in 70% ethanol for at least 2 hours at 4°C. Ethanol-suspended cells were then centrifuged at 200× *g* for 5 minutes and washed twice in PBS to remove residual ethanol. For cell cycle analysis, the pellets were suspended in 1 mL of PBS containing 0.02 mg/mL of propidium iodide, 0.5 mg/mL of DNase-free RNase A and 0.1% of Triton X-100 and incubated at 37°C for 30 minutes. Cell cycle profiles were obtained using a FACScan flow cytometer (Becton Dickinson, San Jose, CA) and data were analyzed by ModFit LT software (Verity Software House, Inc., Topsham, ME).

Apoptosis Assay

To quantify drug-induced apoptosis, annexin V/propidium iodide staining was done followed by flow cytometry. Briefly, after drug treatments (IC_{80} for each drug for 72 hours), both floating and attached cells were combined and subjected to annexin V/propidium iodide staining using annexin V-FITC apoptosis detection kit (Oncogene Research Products, San Diego, CA) according to the protocol provided by the manufacture. Untreated control cells (24–72 hours) were maintained in parallel to the drug-treated group. In cells undergoing apoptosis, annexin V binds to phosphatidylserine, which is translocated from the inner to the outer leaflet of the cytoplasmatic membrane. Double staining is used to distinguish between viable, early apoptotic, and necrotic or late apoptotic cells (16). The resulting fluorescence (FLH-1 channel for green fluorescence and FLH-2 channel for red fluorescence) was measured by flow cytometry using a FACScan flow cytometer (Becton Dickinson). According to this method, the lower left quadrant shows the viable cells, the upper left quadrant shows cell debris, the lower right quadrant shows the early apoptotic cells and the upper right quadrant shows the late apoptotic and necrotic cells.

Animals

Fifty male athymic nude (*nu/nu*) mice (Charles River Laboratories, Wilmington, MA) were used for *in vivo* testing. The animals were fed ad libitum and kept in air-conditioned rooms at 20 ± 2°C with a 12-hour light-dark period. Animal care and manipulation were in agreement with the University of Southern California Institutional Guidelines, which are in accordance with the Guidelines for the Care and Use of Laboratory Animals.

Drug Treatment of Tumor Xenografts

PC3 cells from *in vitro* cell culture were inoculated s.c. in both flanks of athymic nude mice (2×10^6 cells/flank) under aseptic conditions. Tumor growth was assessed by biweekly measurement of tumor diameters with a Vernier caliper (length × width). Tumor weight was calculated according to the formula: TW (mg) = tumor volume (mm^3) = $d^2 \times D/2$, where d and D are the shortest and longest diameters, respectively. Cells were allowed to grow to an average volume of 100 mm^3. Animals were then randomly assigned for control and treatment groups, to receive control vehicle or SC21 (0.3 and 3 mg/kg, dissolved in isotonic saline solution) via i.p injections once a day for 5 days. Treatment of each animal was based on individual body weight. After 5 days of treatment, the tumor volumes in each group were measured once a week for 4 weeks. Treated animals were checked daily for treatment toxicity / mortality. The percentage of tumor growth inhibition was calculated as %T/C = 100 × (mean TW of treated group / mean TW of control group).

Computational ADMET Analysis

Structures of all the compounds were built and minimized in the Catalyst software package (Accelrys, Inc., San Diego, CA). The possible unique conformations for each compound over a 20 kcal/mol energy range were generated using the best conformation generation method within Catconf module of Catalyst. The low-energy conformers of all the compounds were exported to Accord (Accelrys) to calculate A log P 98 and fast polar surface area. The log P values were also calculated with ADMET Predictor (Simulations Plus). The human intestinal absorption plot was constructed using the A log P 98 and the fast polar surface area values of the compounds as previously described (17, 18).

Statistical Analysis

Assays were set up in triplicate and the results were expressed as means ± SD. Statistical analysis and P value determination were done by two-tailed paired t test with a confidence interval of 95% for determination of the significance differences between treatment groups. $P < 0.05$ was considered to be significant. ANOVA was used to test for significance among groups. The SAS statistical software package (SAS Institute, Cary, NC) was used for statistical analysis.

Results

Selection of Compounds Based on Lipinski's Rule-of-Five

From >2,200 compounds selected using pharmacophore modeling, toxicity prediction and clustering, a selection of 950 compounds were evaluated by a 3-(4,5-dimethylthiazol-2-yl)-2,5-diphenyltetrazolium bromide cytotoxicity assay. Eighteen compounds exhibited superior activity profiles against a panel of cancer cell lines from different origins. The structures, physicochemical properties, and cytotoxicities of these compounds are presented in Table 1. All compounds satisfied Lipinski's rule-of-five. This rule was based on an analysis of 2,245 compounds from the World Drug Index database that ~90% of marketed drugs have (*a*) molecular weight <500, (*b*) C log P <5, (*c*) hydrogen bond donors (sum of O-H and N-H) <5, (*d*) hydrogen-bond acceptor (sum of N and O atoms) <10 (19).

All 18 compounds showed IC_{50} values ≤20 μmol/L in either CEM or HEY cells. The range of activity varied >300-fold, with SC26 and SC27 being the most potent (IC_{50} = 0.06 μmol/L) and SC33, SC34, and SC36 the least potent (IC_{50} = 20 μmol/L).

Selection of Compounds Based on Polar Surface Area

From the original studies of Palm et al. (20–22) with a small number of compounds and the more recent studies by Kelder et al. (23) with 1,590 orally administered drugs, it was recommended that a maximum polar surface area value of ~120 Å^2 be for compounds intended to be orally absorbed by passive diffusion. Therefore, compounds with a polar surface area >140 Å^2 would tend to show poor (<10%) absorption, whereas compounds with polar surface area <60 Å^2 could be predicted to show complete (>90%) absorption. Several variants of polar surface area calculations such as dynamic, topological, and fast polar surface area are incorporated in various software packages (24). We used fast polar surface area plots to predict absorption as described (17, 18) and the data are presented in Fig. 1. Compounds that fall in the area shown by the 95% confidence ellipse are expected to have favorable absorption and oral bioavailability. All compounds showed fast polar surface areas of <140 Å^2 and log P value of <5. Therefore, no obvious violations were observed using either the 99% confidence ellipse (outer ellipse) or 95% confidence ellipse (inner ellipse; Fig 1).

SC21 and SC23 Show Remarkable Potency against a Panel of Hormone-Dependent and -Independent Cell Lines

Although many of our original 950 compounds showed favorable calculated physicochemical properties, the 16 compounds presented in Table 1 were among the most potent in our initial screen. On the basis of subsequent testing against drug-resistant cell lines, we selected SC21 and SC23 for further evaluation. The sensitivity of a panel of seven human cancer cell lines to SC21 and SC23 was assessed by a 3-(4,5-dimethylthiazol-2-yl)-2,5-diphenyltetrazolium bromide-assay. Both drugs exhibit a high potency in this panel of cancer cell lines from different tumor origins (Table 2) and exhibited a time- and dose-dependent growth-inhibitory effect (Fig. 2). Thus, *in vitro* cell death increased with increasing concentrations and exposure time of SC21 and SC23.

The activity of both agents was remarkable in prostate cancer cell lines with the exception of PC3 cells, which seemed to be the least sensitive cell line to SC21 and SC23 (IC_{50} value 3.2 ± 0.2 and 2.0 ± 0.5 μmol/L, respectively). The difference in sensitivity to these agents may be independent of the status of androgen receptor (mutated in PC3 and DU145), p53 (null in PC3, mutated in DU145

Table 1. Physicochemical properties and cytotoxicity of salicylhydrazides

Compound	Structure	Molecular weight	HBA	HBD	Rbond	A log *P* 98	Fast polar surface area	IC_{50} (μmol/L)x
SC20	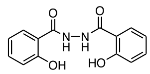	272	6	4	7	1.33 (2.02)	101.8	0.1 ± 0.01
SC21	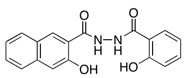	322	6	4	7	2.24 (3.29)	101.8	0.4 ± 0.06
SC22	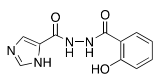	246	7	4	6	0.97 (0.22)	100.1	NT
SC23	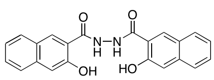	372	6	4	7	3.15 (3.77)	90.9	2.3 ± 0.2
SC24	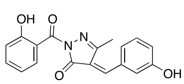	322	6	2	5	2.75 (3.56)	90.9	0.13
SC25	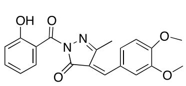	366	7	1	6	2.99 (3.86)	87.9	0.15
SC26	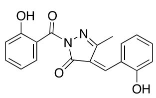	322	6	2	5	2.75 (3.47)	90.9	0.06
SC27	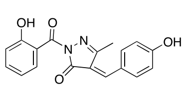	322	6	2	5	2.75 (3.47)	90.9	0.06
SC28	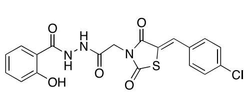	431	8	3	8	2.96 (2.66)	118.9	10 ± 2
SC29	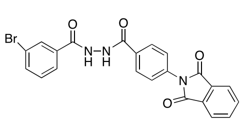	464	7	2	6	3.84 (2.75)	98.17	7 ± 2
SC30	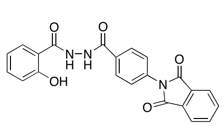	401	8	3	7	2.83 (2.45)	118.99	6.5 ± 1
SC31	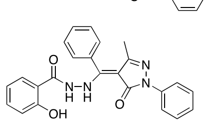	412	7	3	7	3.02 (4.14)	95.71	10 ± 2
SC32	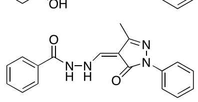	320	6	2	5	1.54 (3.16)	74.89	2 ± 1
SC33	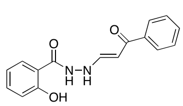	282	5	3	7	1.97 (2.86)	81.03	20 ± 2

(Continued on the following page)

Table 1. Physicochemical properties and cytotoxicity of salicylhydrazides (Cont'd)

Compound	Structure	Molecular weight	HBA	HBD	Rbond	A log *P* 98	Fast polar surface area	IC_{50} (μmol/L)
SC34	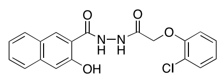	370	6	3	8	3.01 (3.72)	89.9	20 ± 2
SC35	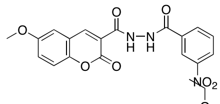	383	9	2	6	1.77 (2.30)	138.20	12 ± 2
SC36	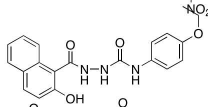	365	7	4	9	2.75 (3.60)	102.77	20 ± 2
SC37	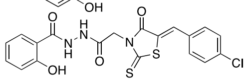	447	6	3	8	3.33 (2.10)	101.69	15 ± 3

NOTE: The IC_{50} values for SC24 to SC27 were determined in CEM cells. All other IC_{50} values are from HEY cells.
Abbreviations: HBA, number of hydrogen bond acceptors; HBD, number of hydrogen bond donors; Rbond, number of rotatable bonds; A log *P* 98, logarithm of the octanol-water partition coefficient [values in parentheses were calculated based on a Simulations Plus model (S + log *P*)].

and wild-type in LNCaP), p21 (mutated in DU145), or p16 (mutated in DU145; Table 2). Interestingly, SC23 exhibits a high potency in pRb-mutated cell lines (DU145 and MDA-MB468).

SC21 and SC23 also showed remarkable potency in the three breast cancer cell lines irrespective of estrogen receptor (ER+ in MCF-7 and MDA-MB-435) and p53 status (mutated in MDA-MB-435 and MDA-MB-468). The activity of SC21 in ovarian tumor–derived cell line HEY was also remarkable considering that this cell line seemed to be practically resistant to cisplatin, the most commonly used drug in ovarian cancer (13, 14). This cell line however seemed to be the least sensitive to SC23.

SC21 Treatment Induces a G_1 and S Phase Cell Cycle Arrest

Cell cycle perturbations induced by SC21 were examined in DU145 and PC3 prostate cancer cells as well as in highly metastatic MDA-MB-435 breast cancer cells and cisplatin-resistant HEY ovarian cancer cells. The analysis of DNA profiles by flow cytometry indicated that SC21 induced cell cycle arrest in G_0/G_1 phase in DU145 (Fig. 3). At 72 hours

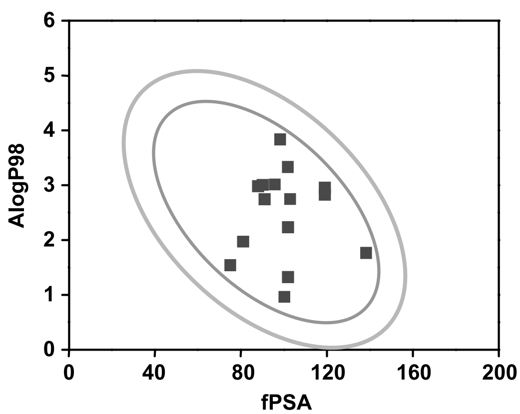

Figure 1. Prediction of drug absorption. Fast polar surface area in $Å^2$ for each compound is plotted against their corresponding calculated partition coefficient. The area encompassed by the ellipse is a prediction of good absorption with no violation of ADMET properties. On the basis of Egan et al. (17) absorption model, the outer ellipse represents a 99% confidence, whereas the inner ellipse a 95% confidence.

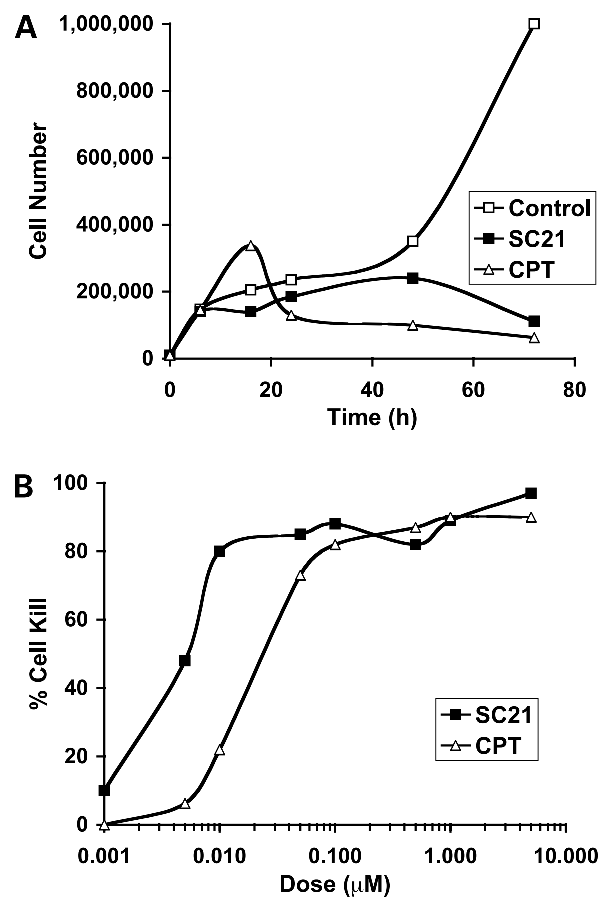

Figure 2. Time- (**A**) and concentration-dependent (**B**) inhibition of DU145 cells by SC21 and CPT.

Table 2. Sensitivity of breast, ovarian, and prostate cancer cell lines to SC21, SC23, and CPT

Cell line	Origin	Hormone receptor	p53	pRb	p16	p21	IC_{50} values (mean ± SD)*		
							SC21 (nmol/L)	SC23 (nmol/L)	CPT (nmol/L)
PC3	prostate	AR−	null	WT	WT	WT	3,250 ± 106	2,000 ± 500	900 ± 210
DU145	prostate	AR−	Mut	null	Mut	Mut	120 ± 50	50 ± 19	25 ± 7
LNCaP	prostate	AR+	WT	WT	WT	WT	200 ± 70	850 ± 200	25 ± 6
HEY	ovarian	AR+	WT	ND	WT	ND	400 ± 60	2,350 ± 212	35 ± 7
MCF-7	breast	ER+	WT	WT	WT	WT	40 ± 7	280 ± 35	30 ± 3
MDA-MB-435	breast	ER−	Mut	WT	WT	WT	35 ± 7	240 ± 28	27 ± 2
MDA-MB-468	breast	ER−	Mut	null	ND	WT	200 ± 2	50 ± 14	100 ± 2

Abbreviations: AR, androgen receptor; ER, estrogen receptor; WT, wild-type; Mut, mutated; ND, not determined.
*Cytotoxic concentration (IC_{50}) is defined as drug concentration causing a 50% decrease in cell population.

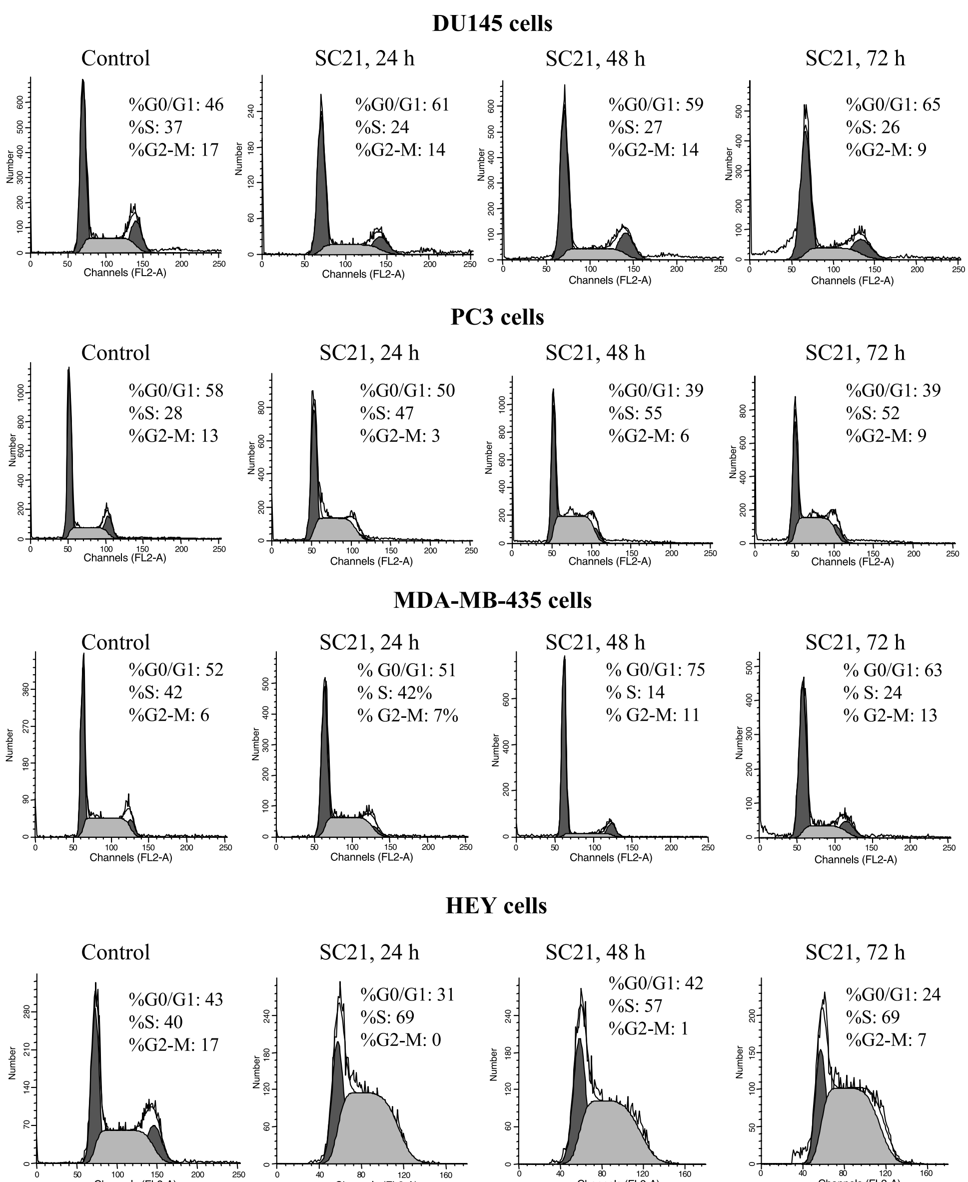

Figure 3. Flow cytometric analysis of the cell cycle profiles of DU145, PC3, MDA-MB-435, and HEY cells treated with SC21. Cells were exposed for 24, 48, and 72 h to SC21 (IC_{50}) then harvested, stained with propidium iodide and analyzed for perturbation in the cell cycle. SC21 induced a G_0/G_1 phase arrest in DU145 and MDA-MB-435 cells and S phase arrest in PC3 and HEY cells. Control cells shown were measured at 24 h and, as expected, no significant changes were observed in the control cells at 48 and 72 h.

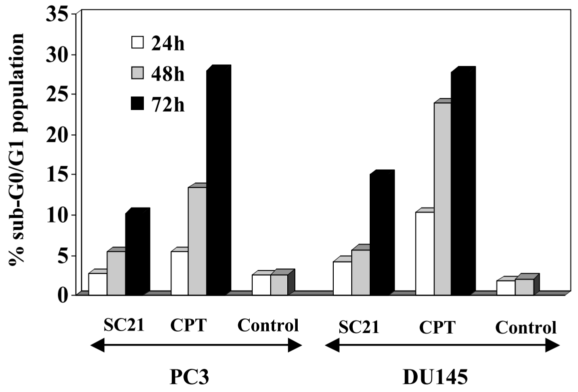

Figure 4. Percentage of apoptosis calculated by measuring sub-G_0/G_1 population using flow cytometry. Apoptotic cell population increased with time in PC3 and DU145 treated with SC21 and CPT.

of exposure to SC21, 65% of the cells were still retained in G_0/G_1 phase compared with 46% in controls. The observed increment in G_0/G_1 was accompanied by a decrease in the number of cells in S and G_2-M phases. Similar effects were obtained on asynchronous breast cancer MDA-MB-435 cells (Fig. 3).

It was noteworthy that SC21 induced S phase arrest in PC3 and HEY cell lines (Fig. 3). SC21 treatment for 72 hours resulted in 52% and 69% accumulation in S phase in PC3 and HEY cells, respectively. The effect observed on both cell lines was comparable to the arrest induced by CPT (data not shown).

The maximum arrest in MDA-MB-435 and PC3 cells was observed at 48 hours of SC21 treatment, which was sustained up to 72 hours. This property of SC21 to induce cell cycle arrest makes it an ideal agent for combination with drugs acting at different stages of cell cycle, such as taxanes.

SC21 Treatment Induces Apoptosis

SC21 and CPT-induced apoptosis was measured by flow cytometry (Fig. 4). SC21 at an IC_{80} dose for 72 hours induced 12% to 15% apoptosis as measured by calculating sub-G_0/G_1 population. CPT resulted in 30% apoptosis under similar conditions (Fig. 4). An early event in apoptotic cell death is the translocation of the phosphatidyl-serine residues to the outer region of the cell membrane. This event precedes nuclear breakdown, DNA fragmentation, the appearance of most apoptosis-associated molecules, and is readily measured by annexin V binding assay. By this method, we compared SC21 with CPT. As shown in Fig. 5, the percentage of early plus late apoptotic cells reached 72% and 59% after 72 hours exposure to SC21 and CPT, respectively.

SC21 Shows *In vivo* Efficacy in Mice Xenograft Models

The *in vivo* efficacy of SC21 was evaluated in nude mice inoculated with human prostate PC3 cells. A schematic outline of the experimental procedure is shown in Fig. 6A. Animals were treated with daily i.p. injections of saline (controls) and SC21 at 0.3 or 3 mg/kg. After 5 days of dosing, the drug treatment was discontinued and the animals were monitored biweekly for 5 weeks. Figure 6B shows the volume (mean ± SD) for SC21-treated PC3 xenografts over time. SC21 significantly reduced tumor burden in prostate xenografts (Fig. 6C) without apparent toxicity. Treatment with SC21 was well-tolerated and did not result in any drug-related deaths and changes in body weight. The untreated control mice had an average weight of 33.2 ± 1.45 g before the experiments and 34.3 ± 2.79 g after the experiment. Mice treated with 0.3 mg/kg of SC21 had an average weight of 32.1 ± 1.92 g and mice treated with 3.0 mg/kg of SC21 had an average weight of 33.3 ± 1.89 g.

Discussion

Using pharmacophore models to distinguish antiviral compounds from anticancer compounds, we have successfully identified a new class of leads with remarkable activity profiles both *in vitro* and *in vivo*. Two members of this new class of compounds, SC21 and SC23, were

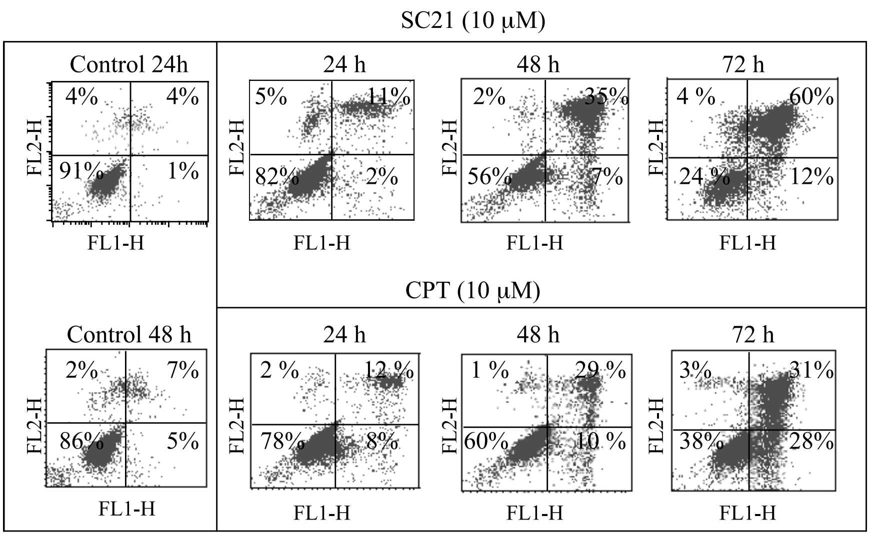

Figure 5. Apoptosis analysis of DU145 cells treated with SC21 or CPT (IC_{80}). Cells were treated with SC21 or CPT for 24, 48, and 72 h, harvested, stained with annexin V/propidium iodide and analyzed by flow cytometry. Untreated control cells (24 and 48 h) were also included in the analysis. Annexin V-FITC signals are recorded in FL1-H or red channel and propidium iodide in FL2-H or green channel. Cells in the bottom left quadrant (annexin V-negative, propidium iodide-negative) are viable, whereas cells in the right quadrant (annexin V-positive, propidium iodide-negative) are in the early stages of apoptosis, and the cells in the top right quadrant (annexin V-positive, propidium iodide-positive) are in later stages of apoptosis and necrosis.

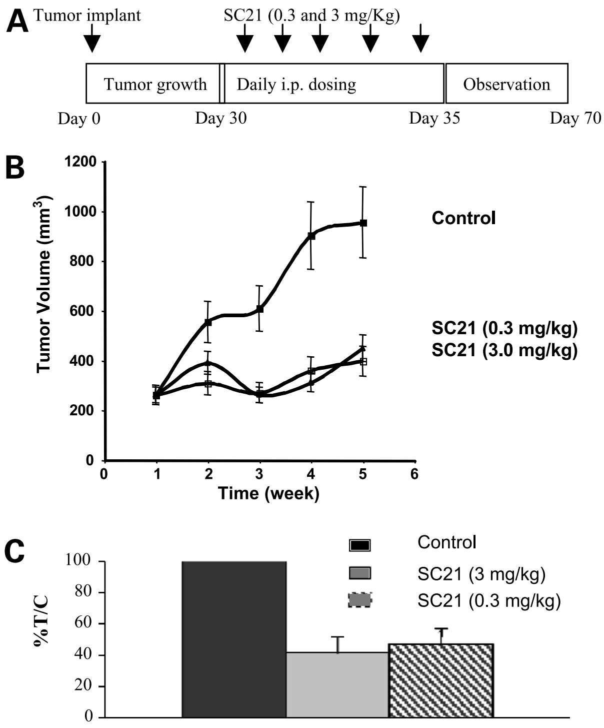

Figure 6. **A,** schematic outline of tumor growth and dosing in PC3 mice xenografts. **B,** SC21 reduced the size of human prostate cancer xenografts. Athymic nude mice implanted with PC3 cells were treated with the indicated concentration of SC21 through daily i.p. administration for 5 d. Tumor growth was monitored for 5 wks. Values represent the tumor weight (mean ± SD) for each group. **C,** dose-response to SC21 in the PC3 xenograft. Values represent the %T/C from each treatment group on the last day of measurement (after 5 wks); *bars*, ± SD. Treatment with SC21 significantly reduced tumor growth (%T/C ≤50%) at both doses as compared with the control.

evaluated further against a range of human tumor-derived cancer cell lines. Both compounds inhibited cell growth in a time- and dose-dependent manner. The efficacy of SC21 and SC23 in prostate cancer cells was comparable to that of CPT and their cytotoxic effects may be independent of the androgen receptor, p53, p21, and p16 status. Interestingly, defects in pRb expression seemed to confer higher sensitivity to SC23 in DU145 and MDA-MB-468 cell lines. SC21 seemed to be 16- to 90-fold more potent in ER+ and ER− breast cancer cells as compared with PC3 prostate cancer cells, suggesting that this compound might be a potential candidate for the treatment of hormone receptor–positive and -negative breast cancers.

Consistent with the effect of SC21 on cell growth inhibition, our data also show the ability of this compound to arrest cell cycle progression. This property of SC21 opens the possibility to investigate innovative combinations with other agents acting at different stages of the cell cycle, such as taxanes. Notably, the different cell lines used in the present study displayed different cell cycle perturbations following SC21 treatment. SC21 arrested DU145 and MDA-MB-435 cells in G_0/G_1 phase, and PC3 and HEY cells in S phase. Previously, similar observations reported with different drugs were attributed to different cell cycle checkpoint status and susceptibility to apoptosis (25–27). It is well-established that p53 plays a major role on cell cycle retention in G_0/G_1 phase. We can conclude that the cell cycle arrest induced by SC21 in these cell lines may be independent of the p53 status (mutated in DU145, null in PC3). Further studies using various p53 mutant and p53 null cell lines are required to better understand the role of p53 in response to SC21 treatment.

It is known that apoptosis-signaling pathways and cellular events controlling them, have a profound effect both on cancer progression and in response to chemoherapy (28–31). Based on annexin V/propidium iodide staining and sub-G_0/G_1 fractions, it is clear that SC21 activity is mediated by apoptosis in a fashion comparable to that of CPT. SC21 also showed *in vivo* antitumor efficacy against PC3 tumor xenografts. Significant reduction in tumor growth was found for all doses tested. Furthermore, SC21 was well-tolerated and did not result in drug-related deaths. Finally, the fact that SC21 exhibited *in vivo* efficacy against the PC3 prostate cancer xenografts despite PC3 cells being the least sensitive *in vitro* model, clearly show its potential as a novel anticancer agent. Studies including other models such as breast and lung cancer are currently in progress.

In conclusion, considering their cytotoxicity profiles in a variety of *in vitro* systems, including different cell lines having intrinsic or acquired resistance to known drugs, and their favorable *in vivo* properties, salicylhydrazides seem to represent a novel class of anticancer drugs that function by a new mechanism of action. These agents could have promising therapeutic potential. Proteomic studies are currently under way to better understand the mechanisms involved in the activity of salicylhydrazides.

References

1. Neamati N, Barchi JJ Jr. New paradigms in drug design and discovery. Curr Top Med Chem 2002;2:211 – 27.

2. Hong H, Neamati N, Wang S, et al. Discovery of HIV-1 integrase inhibitors by pharmacophore searching. J Med Chem 1997;40:930 – 6.

3. Zhao H, Neamati N, Sunder S, et al. Hydrazide-containing inhibitors of HIV-1 integrase. J Med Chem 1997;40:937 – 41.

4. Neamati N, Hong H, Owen JM, et al. Salicylhydrazine-containing inhibitors of HIV-1 integrase: implication for a selective chelation in the integrase active site. J Med Chem 1998;41:3202 – 9.

5. Neamati N, Lin Z, Karki RG, et al. Metal-dependent inhibition of HIV-1 integrase. J Med Chem 2002;45:5661 – 70.

6. Fesen MR, Kohn KW, Leteurtre F, Pommier Y. Inhibitors of human immunodeficiency virus integrase. Proc Natl Acad Sci U S A 1993;90: 2399 – 403.

7. Neamati N, Mazumder A, Sunder S, Lown JW, Pommier Y. Lexitropsins as potent inhibitors of HIV-1 integrase. In Keystone Symposia on Molecular and Cellular Biology; 1997; Santa Fe. Keystone Symposia; 1997. p. 32.

8. Neamati N, Hong H, Sunder S, Milne GW, Pommier Y. Potent inhibitors of human immunodeficiency virus type 1 integrase: identification of a novel four-point pharmacophore and tetracyclines as novel inhibitors. Mol Pharmacol 1997;52:1041 – 55.

9. Neamati N, Hong H, Mazumder A, et al. Depsides and depsidones as inhibitors of HIV-1 integrase: discovery of novel inhibitors through 3D database searching. J Med Chem 1997;40:942 – 51.

10. Melek M, Jones JM, O'Dea MH, et al. Effect of HIV integrase inhibitors on the RAG1/2 recombinase. Proc Natl Acad Sci U S A 2002;99: 134 – 7.

11. Neamati N, Marchand C, Pommier Y. HIV-1 integrase inhibitors: past, present, and future. Adv Pharmacol 2000;49:147 – 65.

12. Rice P, Craigie R, Davies DR. Retroviral integrases and their cousins. Curr Opin Struct Biol 1996;6:76 – 83.

13. Buick RN, Pullano R, Trent JM. Comparative properties of five human ovarian adenocarcinoma cell lines. Cancer Res 1985;45:3668 – 76.

14. Hamaguchi K, Godwin AK, Yakushiji M, et al. Cross-resistance to diverse drugs is associated with primary cisplatin resistance in ovarian cancer cell lines. Cancer Res 1993;53:5225 – 32.

15. Carmichael J, DeGraff WG, Gazdar AF, Minna JD, Mitchell JB. Evaluation of a tetrazolium-based semiautomated colorimetric assay: assessment of chemosensitivity testing. Cancer Res 1987;47:936 – 42.

16. Fadok VA, Voelker DR, Campbell PA, et al. Exposure of phosphatidylserine on the surface of apoptotic lymphocytes triggers specific recognition and removal by macrophages. J Immunol 1992;148: 2207 – 16.

17. Egan WJ, Merz KM Jr, Baldwin JJ. Prediction of drug absorption using multivariate statistics. J Med Chem 2000;43:3867 – 77.

18. Egan WJ, Lauri G. Prediction of intestinal permeability. Adv Drug Deliv Rev 2002;54:273 – 89.

19. Lipinski CA, Lombardo F, Dominy BW, Feeney PJ. Experimental and computational approaches to estimate solubility and permeability in drug discovery. Adv Drug Deliv Rev 1997;23:3 – 25.

20. Palm K, Luthman K, Ungell AL, et al. Evaluation of dynamic polar molecular surface area as predictor of drug absorption: comparison with other computational and experimental predictors. J Med Chem 1998;41: 5382 – 92.

21. Palm K, Stenberg P, Luthman K, Artursson P. Polar molecular surface properties predict the intestinal absorption of drugs in humans. Pharm Res 1997;14:568 – 71.

22. Palm K, Luthman K, Ungell AL, Strandlund G, Artursson P. Correlation of drug absorption with molecular surface properties. J Pharm Sci 1996;85:32 – 9.

23. Kelder J, Grootenhuis PD, Bayada DM, Delbressine LP, Ploemen JP. Polar molecular surface as a dominating determinant for oral absorption and brain penetration of drugs. Pharm Res 1999;16:1514 – 9.

24. Clark DE, Grootenhuis PD. Predicting passive transport in silico—history, hype, hope. Curr Top Med Chem 2003;3:1193 – 203.

25. Zuco V, Supino R, De Cesare M, et al. Cellular bases of the antitumor activity of a 7-substituted camptothecin in hormone-refractory human prostate carcinoma models. Biochem Pharmacol 2003;65:1281 – 94.

26. Schiff PB, Horwitz SB. Taxol stabilizes microtubules in mouse fibroblast cells. Proc Natl Acad Sci U S A 1980;77:1561 – 5.

27. Lanzi C, Cassinelli G, Cuccuru G, et al. Cell cycle checkpoint efficiency and cellular response to paclitaxel in prostate cancer cells. Prostate 2001;48:254 – 64.

28. Sun SY, Hail N Jr, Lotan R. Apoptosis as a novel target for cancer chemoprevention. J Natl Cancer Inst 2004;96:662 – 72.

29. Assuncao Guimaraes C, Linden R. Programmed cell deaths. Apoptosis and alternative deathstyles. Eur J Biochem 2004;271:1638 – 50.

30. Pommier Y, Sordet O, Antony S, Hayward RL, Kohn KW. Apoptosis defects and chemotherapy resistance: molecular interaction maps and networks. Oncogene 2004;23:2934 – 49.

31. Norbury CJ, Zhivotovsky B. DNA damage-induced apoptosis. Oncogene 2004;23:2797 – 808.

Discovery and preclinical evaluation of a novel class of small-molecule compounds in hormone-dependent and -independent cancer cell lines

Carmen Plasencia, Raveendra Dayam, Qingcai Wang, et al.

Mol Cancer Ther 2005;4:1105-1113.